Nonlinear Control and Design Methodologies for

Electrostatic MEMS Devices

Except where reference is made to the work of others, the work described in this thesis is my own or was done in collaboration with my advisory committee. This thesis does not include proprietary or classified information.

Phillip M. Ozmun

Certificate of Approval:

Ramesh Ramadoss Assistant Professor Electrical and Computer Engineering	John Y. Hung, Chair Professor Electrical and Computer Engineering
Robert N. Dean Assistant Professor Electrical and Computer Engineering	Joe F. Pittman Interim Dean Graduate School

Nonlinear Control and Design Methodologies for Electrostatic MEMS Devices

Phillip M. Ozmun

A Thesis

Submitted to

the Graduate Faculty of

Auburn University

in Partial Fulfillment of the

Requirements for the

Degree of

Master of Science

Auburn, Alabama
August 04, 2007

Nonlinear Control and Design Methodologies for

Electrostatic MEMS Devices

Phillip M. Ozmun

Permission is granted to Auburn University to make copies of this thesis at its discretion, upon the request of individuals or institutions and at their expense. The author reserves all publication rights.

Signature of Author

Date of Graduation

Vita

Phillip was born on December 4, 1979 in South-Eastern Idaho to Michael and Joan Ozmun. After graduating from Idaho Falls High School, he continued his education at the University of Idaho. While earning his B.S. degree in Mechanical Engineering he enjoyed socializing with friends and playing on the university's club baseball team. After graduation he worked for Havlovick Engineering Services in Mobile, Alabama. After the projects he worked on in Mobile were completed, he pursued graduate work at Auburn University.

Thesis Abstract

Nonlinear Control and Design Methodologies for Electrostatic MEMS Devices

Phillip M. Ozmun

Master of Science, August 04, 2007
(B.S.M.E, University of Idaho, 2003)

62 Typed Pages

Directed by John Y. Hung

A method to extend the travel range of electrostatically actuated MEMS is presented. A gap closing actuator (GCA) is used to demonstrate the method. An output (position) feedback controller is presented, along with two variable structure controllers. The forced-damping variable structure controller uses two stable structures, and the sliding mode (hybrid) controller uses an unstable structure and a stable structure. An adaptive controller is also presented for devices that have adequate natural damping. A design methodology for nonlinear mechanical springs is presented. The mechanical nonlinearity offsets the electrostatic nonlinearity to extend the device travel range without feedback.

Acknowledgments

First and foremost, I must thank my parents for all their encouragement. Without their support, it is unlikely I would have ever received my bachelor's degree in Mechanical Engineering at the University of Idaho.

Next, I'd like to thank Bradley Havlovick and Jim Richardson at Havlovick Engineering Services. Their expertise, guidance, and patience helped me develop as an engineer, and the experience I gained working with them will stay with me the rest of my career.

I must also thank Dr. John Y. Hung, my adviser, without whose direction and assistance, I could have never completed my degree. His control courses were some of the most informative and stimulating classes I have taken.

Working with Dr. Ramesh Ramadoss was also an integral part of my Auburn experience. His guidance and knowledge in the area of MEMS was instrumental in the formulation of the method developed in this thesis.

Style manual or journal used Bibliography conforms to those in the IEEE Transactions.

Computer software used The document preparation package TEX (specifically LATEX) together with the departmental style-file `aums.sty`.

Table of Contents

List of Figures x

1 Introduction 1
1.1 Chapter Overview . . . 2
1.1.1 Chapter 1: Introduction . . . 2
1.1.2 Chapter 2: Variable Structure Technique . . . 2
1.1.3 Chapter 3: Adaptive Controller . . . 2
1.1.4 Chapter 4: Device Function Design . . . 3
1.1.5 Chapter 5: Extension to Other Systems . . . 3
1.2 Nonlinear Electrostatic MEMS Actuators . . . 3
1.3 Governing Equations . . . 4
1.4 Previous Research . . . 5
1.5 Governing Equation . . . 6
1.6 Input and Device Functions . . . 7
1.7 Static Analysis: Equilibrium and Stability . . . 9
1.7.1 Open Loop Considerations . . . 10
1.7.2 Closed Loop Considerations . . . 11
1.8 Dynamic Analysis: Equilibrium and Stability . . . 12
1.8.1 Static Force Plots . . . 12
1.8.2 Force Potential Barriers . . . 13
1.9 Design of a Linear Controller . . . 14
1.9.1 Satisfying Device-Input Static Requirements . . . 15
1.9.2 Positive Region Operation . . . 16
1.9.3 Negative Region Operation . . . 17
1.9.4 χ's Effect on Localized Stiffness . . . 19

2 Variable Structure Technique 21
2.1 Available Structures . . . 23
2.2 GCA Variable Structure Controllers . . . 23
2.2.1 Stable-Stable (Forced Damping) Switching . . . 24
2.2.2 Stable-Unstable (Sliding Mode) Switching . . . 26
2.2.3 Switching Surface Considerations . . . 28

3 Adaptive Controller 29
3.1 Robustness Comparison . . . 32

4 Device Function Design 34
4.1 Nonlinear Springs 35
4.2 Implementation Issues 37

5 Extension to Other Systems 40
5.1 Series Capacitor Method 40
5.2 Torsional Devices 42

6 Conclusion and Discussion 46
6.1 Overview 46
6.2 Output vs State Feedback 48
6.3 Multi-Dimensional Actuators 48
6.4 Final Discussion 49

Bibliography 50

List of Figures

1.1 Gap Closing Actuator 7

1.2 Device Function 8

1.3 Device and Input Functions in Open Loop 11

1.4 Device and Input Functions with Closed Loop 12

1.5 Net Force Function for Fig 2.4 13

1.6 Energy Barriers for Dynamic Stability 14

1.7 Output Position for Linear Controller, Positive Region 16

1.8 Input Voltage for Linear Controller, Positive Region 17

1.9 Output Position for Linear Controller, Negative Region 18

1.10 Input Voltage for Linear Controller, Negative Region 18

1.11 Device-Input Function for Various Chi Values 19

1.12 Net Force Functions for Various Chi Values 20

2.1 Low Stiffness Phase Portrait 21

2.2 High Stiffness Phase Portrait 22

2.3 Mixed System Phase Portrait 22

2.4 Constant Voltage, Zero Damping Phase Portrait 23

2.5 Stable-Stable Phase Portrait 24

2.6 Stable-Stable: Position vs Time 25

2.7 Stable-Stable: Control Voltage vs Time 25

2.8 Stable-Unstable Phase Portrait 26

2.9 Stable-Unstable: Postion vs Time 27
2.10 Stable-Unstable: Control Voltage vs Time 27
3.1 Adaptive Controller Phase Portrait 30
3.2 Adaptive Controller: Position vs Time 31
3.3 Adaptive Controller: Control Voltage vs Time 31
3.4 Robustness Study: Position vs Time 32
3.5 Robustness Study: Phase Portrait 33
4.1 System Response with Nonlinear Spring 36
4.2 Beam Element for Nonlinear Spring Design 37
4.3 Interference and Deflection Profiles 38
4.4 Discrete Nonlinear Spring Device Function 39
5.1 Series Capacitor Device-Input Plot 41
5.2 Series Capacitor Net Force Plot 42
5.3 Torsional Device-Input Plot: Open Loop 44
5.4 Net Torque Plot: Open Loop 44
5.5 Torsional Device-Input Plot: Closed Loop 45
5.6 Net Torque Plot: Closed Loop 45

Chapter 1

Introduction

Micro-Electro Mechanical Systems or MEMS devices combine sensors, actuators, mechanical structures, electronics, and optics on a single substrate and combine technological advances from fields that were previously unrelated, such as biology and microelectronics [1]. MEMS have the advantage of being smaller, having a higher Q, low insertion loss, and lower power consumption compared to traditional construction, among several other advantages [2].

MEMS actuators can be driven a multitude of ways. Thermal, piezoelectric, and electrostatic are the most common. In electrostatic actuation there are two classes, linear actuators and nonlinear actuators. In linear actuators the electrostatic force is only dependent on the drive voltage. In nonlinear devices, the electrostatic force varies nonlinearly with respect to position. These nonlinear devices are the focus of this thesis. For a typical device the actuation range in open loop operation is limited to a fraction of the potential range due to a phenomenon called "pull-in", where the nonlinear electrostatic force overwhelms the mechanical spring force. Although research has been performed to extend this travel range by eliminating pull-in there are still physical limitations [3]. Nonlinear electrostatic MEMS devices can be used in the communication industry to replace traditional switches, varactors, phase shifters, filters, and resonators. They also have potential in many optical applications and are currently being used in high definition televisions.

1.1 Chapter Overview

1.1.1 Chapter 1: Introduction

The first sections in chapter 1 cover the governing equations of nonlinear electrostatic MEMS devices, introduce the device-input formulation for such systems, and review some of the previous research done to improve the performance of such devices.

The last sections in chapter 1 apply the device-input formulation to a gap closing actuator (GCA). Static stability (force balance) is used to determine the slope-intersection requirements of the device-input functions to ensure stability. Input function design considerations are covered and a simple, linear controller is proposed. Lastly, an analysis is presented that illustrates how modifying the linear controller gains can modify the local stiffness of the system.

1.1.2 Chapter 2: Variable Structure Technique

Chapter 2 covers two variable structure techniques applied to the GCA using the linear controller from chapter 1. The first technique is based on switching between two stable structures with varying stiffness. The second technique is based on stable-unstable switching, and forms a sliding mode under certain circumstances. The two variable structure controllers are shown to improve the dynamic performance of the GCA system, even in the absence of natural damping.

1.1.3 Chapter 3: Adaptive Controller

Chapter 3 introduces an adaptive technique based on the GCA system and linear controller from chapter 1. A proportional-integral (PI) method is used to adjust the slope

gain of the linear controller. This chapter concludes with a robustness analysis of the controllers presented in chapters 2 and 3.

1.1.4 Chapter 4: Device Function Design

The first 3 chapters were concerned with modifying the input function to improve device performance. Chapter 4 looks at how the device function can be modified to improve system performance. The first section explores design considerations for closed loop operation. Next, a nonlinear mechanical force equation is determined that allows for full range operation without feedback. The nonlinearity is introduced using an interference profile that limits beam deflection. A beam analysis method is proposed for determining the interference profile required.

1.1.5 Chapter 5: Extension to Other Systems

Chapter 5 shows the utility of the method by showing how it can be applied to other nonlinear MEMS. The method is used to demonstrate how the series capacitor method can be used to extend the travel range of the GCA at the cost of higher actuation voltage. Next the method is applied to a torsional device, with similar conclusions to that of the GCA example.

1.2 Nonlinear Electrostatic MEMS Actuators

Electrostatic MEMS actuators can be divided into two types, linear and nonlinear. For both cases the electrostatic force is determined by the energy-displacement relationship associated with the device capacitance:

$$F_e(x) = \frac{1}{2}V^2 \frac{d}{dx}C(x) \tag{1.1}$$

For linear devices like comb-drive actuators the capacitance varies linearly with displacement so that the electrostatic force is independent of displacement. For nonlinear devices the capacitance is inversely proportional to displacement so that the electrostatic force contains inverse-squared terms.

1.3 Governing Equations

A generalized form of the governing equation for all electrostatic MEMS devices is given.

$$m\ddot{x} + b(x, \dot{x})\dot{x} + k(x, \dot{x})x = f_0(x)V(x, \dot{x})^2 \tag{1.2}$$

Where x is the dependent variable (position or rotation), m is a constant inertia term, b is the damping term, k is the spring term, f_0 is an input term, and V is the input voltage. In systems with multiple degrees of freedom, equations in the form of (1.2) typically apply to each DOF.

In the bulk of this thesis, the idea of force balance or static equilibrium is employed regularly. Equation (1.2) can be expressed under steady state equilibrium as the intersection of two curves.

$$f_e(x, \dot{x}) \stackrel{def}{=} V(x, \dot{x})^2 \tag{1.3}$$

$$f_d(x, \dot{x}) \stackrel{def}{=} \frac{k(x, \dot{x})x}{f_0(x)} \tag{1.4}$$

$$f_e(x, \dot{x}) = f_d(x, \dot{x}) \tag{1.5}$$

Where f_e is defined as the feedback or input function of the system. In open loop it is the constant value of the input voltage squared, V^2. The second function, f_d, can be defined as the device function, and is determined by device geometry and material. By manipulating these two functions, devices and controllers can be designed to perform as required.

1.4 Previous Research

As MEMS technology has developed many control and design methodologies have developed to improve performance. Feedback control was first introduced in MEMS sensors in order to enhance measurement accuracy. In some cases designers modified the open-loop control signals using dynamic models. These pre-shaped control methods improved the dynamic behavior without the need of feedback but are highly tailored to each device, have limited application range, and require accurate models [4].

Various geometrical methods have also been researched. These fall mostly into two categories; multiple electrode arrangements [5] and leveraged bending methods [6]. While these methods have their benefits, complications can arise due to complex control and switching requirements for a large number of electrodes, and high actuation voltage using leveraged bending. Closely related to leveraged bending is the use of strain-stiffening springs

to increase travel range. This effect introduces a mechanical nonlinearity to compensate for the electrical nonlinearity that causes pull-in. Current methods rely on residual axial stresses in the mechanical springs and are highly problematic.

A wide variety of feedback techniques have been proposed. Some of the more popular methods include capacitor feedback, current/charge control [7] (also an open loop method), and voltage controllers [4]. Force balance methods have also been used in designing feedback algorithms in micro-mirrors [8]. Traditional nonlinear techniques have also been explored [9]. Force balance techniques were also the basis for the method discussed here. Original developments concerned bi-directional operation of a GCA fabricated at Auburn University [10].

In order to familiarize the reader with the control methodology being used, the technique will be demonstrated on a gap closing actuator (GCA) comprised of interlocked comb-like structures. Figure 1.1 shows the device layout along with sign conventions.

As a voltage is applied across the moving and stationary combs an electrostatic force moves the actuator in the positive x direction. A balancing mechanical spring force acts in the opposite direction if the actuator is in static equilibrium.

1.5 Governing Equation

The dynamic model of the GCA system is given by:

$$m\ddot{x} = -B\dot{x} - Kx + \frac{\epsilon_o \epsilon_r A V^2}{2}\left(\frac{1}{(x_o - x)^2} - \frac{1}{(y_o + x)^2}\right) \tag{1.6}$$

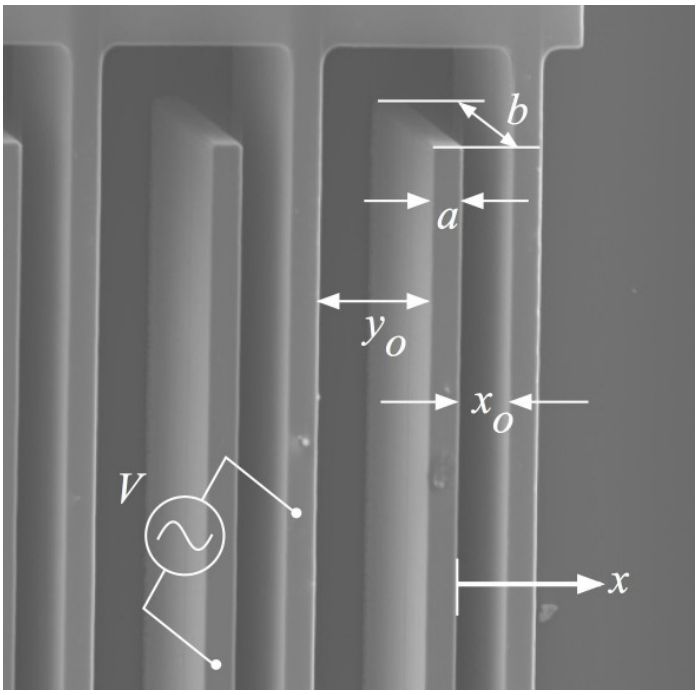

Figure 1.1: Gap Closing Actuator

Where m is the proof mass, B is the damping constant, ϵ_o is the free-space permittivity, ϵ_r is the relative permittivity of air, A is the actuator area, V is the applied voltage, x_o is the nominal positive gap distance, y_o is the nominal negative gap distance, and K is the system spring constant. Values of model parameters are shown in Table 1.1.

1.6 Input and Device Functions

By rewriting the force equation under static equilibrium, the following is observed:

$$V^2(x) = \frac{2Kx}{\epsilon_o \epsilon_r A}\left(\frac{1}{(x_o - x)^2} - \frac{1}{(y_o + x)^2}\right)^{-1} \tag{1.7}$$

$$f_e(x) = f_d(x)$$

Table 1.1: Nomenclature and parameter values

Variable	**Parameter**	**Value**	**Units**
m	mass	3.6519×10^{-7}	kg
B	damping	2.45×10^{-4}	N-sec/m
ϵ_o	free space permittivity	8.854×10^{-12}	F/m
ϵ_r	relative permittivity	1	NA
A	area	5.85×10^{6}	μm^2
x_o	nominal small gap	10	μm
y_o	nominal large gap	25	μm
K	spring constant	103.125	N/m

The left hand side of (1.7) is the input function, and is referred to as $f_e(x)$. The right hand side of (1.7) is the device function, and is referred to as $f_d(x)$. The intersection(s) of these two functions are the locations of the equilibrium points occurring in the travel region. Figure 1.2 shows the device function for the given device. The input function is arbitrary and is not shown; however for a constant voltage, it would be a horizontal line.

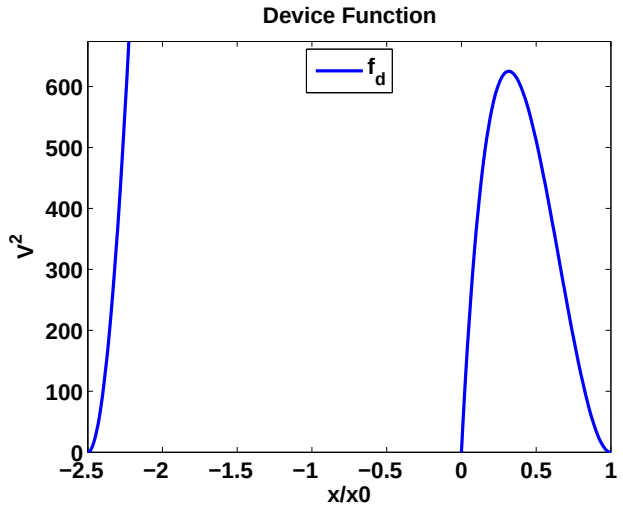

Figure 1.2: Device Function

1.7 Static Analysis: Equilibrium and Stability

Stability of equilibrium points can be determined by examining properties of $f_e(x)$ and $f_d(x)$. By looking at the net force vs. displacement graph, the equilibrium points are located where the net force is equal to zero ($F_{net} = 0$). The stable equilibrium points are equilibrium points that have negative slopes ($\frac{d}{dx}F_{net} < 0$). This implies that a perturbation in one direction yields a net force in the opposite direction to push the actuator back toward the equilibrium point. Requirements for the static stability of the system can be expressed in terms of $f_e(x)$ and $f_d(x)$.

$$F_{net} = \frac{\epsilon_o \epsilon_r A}{2} \left(\frac{1}{(x_o - x)^2} - \frac{1}{(y_o + x)^2} \right) V^2 - Kx \tag{1.8}$$

$$F_{net} = \frac{\epsilon_o \epsilon_r A}{2} \left(\frac{1}{(x_o - x)^2} - \frac{1}{(y_o + x)^2} \right) \ (f_e - f_d) \tag{1.9}$$

Isolating $(f_e - f_d)$ to one side of the equation and taking the derivative with respect to x:

$$\begin{aligned} \frac{d}{dx}(f_e - f_d) = \frac{dF_{net}}{dx} \frac{2}{\epsilon_o \epsilon_r A} \left(\frac{1}{(x_o - x)^2} - \frac{1}{(y_o + x)^2} \right)^{-1} + \\ F_{net} \frac{2}{\epsilon_o \epsilon_r A} \frac{d}{dx} \left(\frac{1}{(x_o - x)^2} - \frac{1}{(y_o + x)^2} \right)^{-1} \end{aligned} \tag{1.10}$$

Since the net force is zero at an equilibrium point and $\frac{d}{dx}F_{net} < 0$, equation (1.10) can be simplified to the following.

$$\frac{d}{dx}(f_e - f_d)\left(\frac{1}{(x_o - x)^2} - \frac{1}{(y_o + x)^2}\right) < 0 \tag{1.11}$$

The sign of the augmenting function depends on the value of x, but can easily be determined, yielding the following result:

For

$$x < \frac{x_o^2 - y_o^2}{2(y_o + x_o)} \rightarrow \frac{d}{dx}(f_e - f_d) > 0$$

For

$$x > \frac{x_o^2 - y_o^2}{2(y_o + x_o)} \rightarrow \frac{d}{dx}(f_e - f_d) < 0$$

So for equilibrium points in the positive region of motion to be stable, $\frac{df_d}{dx} > \frac{df_e}{dx}$, for equilibrium points in the negative region to be stable, $\frac{df_e}{dx} > \frac{df_d}{dx}$.

1.7.1 Open Loop Considerations

During open loop operation the input function is constant with respect to displacement. Because $\frac{df_e}{dx} = 0$, the only stable equilibrium points exist in the positive operation range where the slope of the device function is greater than zero. Figure 1.3 shows the positions of the equilibrium points and how they move with increasing voltage input.

When a voltage is applied, two equilibrium points are formed in the positive range of motion. As the voltage increases, these stable and unstable equilibrium points gravitate

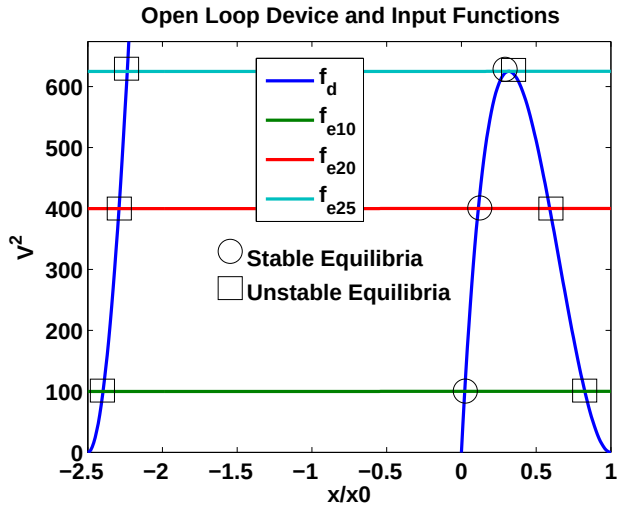

Figure 1.3: Device and Input Functions in Open Loop

toward each other and combine into an unstable equilibrium point when $\frac{df_d}{dx} = 0$, resulting in pull-in.

1.7.2 Closed Loop Considerations

One method of extending the travel range of the device is to employ feedback to the system by forcing the voltage to be a function of x. Figure 1.4 shows the stable and unstable equilibrium points for the device with an arbitrary periodic input function.

Regardless of the input function, the equilibrium voltage is always on the device function curve. The equilibrium points are where the input function intersects the device function, and the slopes of the two functions at those points determine whether the points are stable or unstable. In theory, the device range is the entire gap distance in the positive direction. In the negative direction no equilibrium points can exist where the device function

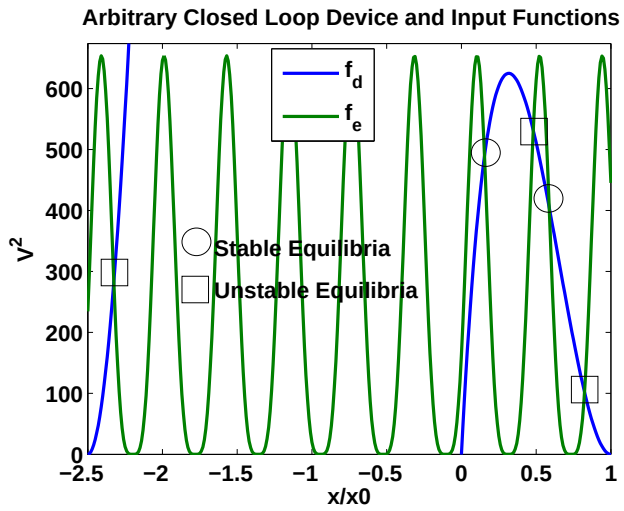

Figure 1.4: Device and Input Functions with Closed Loop

is negative ($0 > x > \frac{x_o^2 - y_o^2}{2(y_o + x_o)}$). Otherwise travel is possible throughout the negative region with proper feedback.

1.8 Dynamic Analysis: Equilibrium and Stability

In general, by knowing the device function one can determine the required input function to establish a stable equilibrium point in the regions described (anywhere in the positive direction, in a limited range in the negative direction). However, it is helpful to understand the dynamics of the system in order to design an adequate input function.

1.8.1 Static Force Plots

Static equilibrium has been the heart of the analysis, so examining the net force plots is insightful. Figure 1.5 shows the net force plot for the feedback function in Figure 1.4. Only the positive region is shown for clarity.

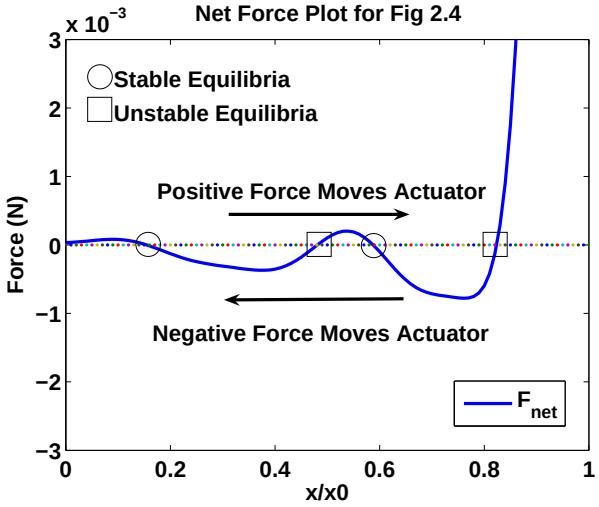

Figure 1.5: Net Force Function for Fig 2.4

Figure 1.5 gives a rough picture of the dynamic stability of the system. Near the stable equilibrium points exist regions of positive and negative force that drive the system back toward the equilibrium point. In these regions the system can oscillate about the equilibrium point as long as there is insufficient energy to reach an adjacent (unstable) equilibrium point. Dynamic stability is limited by these unstable equilibria.

1.8.2 Force Potential Barriers

The area bounded under the force curve is a measure of the electro-mechanical potential energy in the system, similar to the spring potential energy in a mechanical system. Neglecting any damping, all this potential energy is converted to kinetic energy of the moving mass. Figure 1.6 is given for an example.

Initially the actuator is at rest at a stable equilibrium point with potential barriers E_r and E_l to the right and left of the equilibrium point respectively. If the actuator is

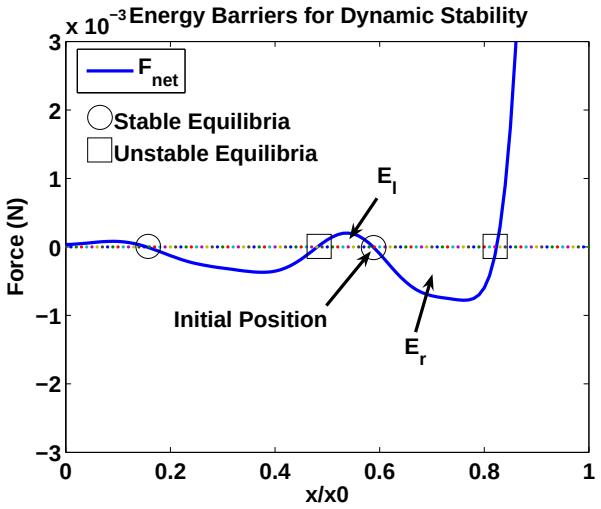

Figure 1.6: Energy Barriers for Dynamic Stability

perturbed with an energy less than either barrier, it will oscillate about the equilibrium point as the energy is converted back and forth between the kinetic energy of the mass and the potential energy of the field. However, if the actuator is perturbed with an energy greater than either barrier, it will leave the region of the current equilibrium point.

In designing an input function the position of the unstable equilibrium points and the potential barriers need to be taken into account to avoid problems associated with the dynamic stability of the system.

1.9 Design of a Linear Controller

A linear controller can be designed to meet the desired criteria. The general form of the feedback function is:

$$V(x) = \Psi(x - \chi) \tag{1.12}$$

Where Ψ is the slope and χ is the x-intercept.

1.9.1 Satisfying Device-Input Static Requirements

In order to establish the desired equilibrium point, the device and input function are equated at the desired point.

$$(\Psi(x_e - \chi))^2 = \frac{2Kx_e}{\epsilon_o \epsilon_r A} \left(\frac{1}{(x_o - x_e)^2} - \frac{1}{(y_o + x_e)^2} \right)^{-1} \tag{1.13}$$

Solving for Ψ:

$$\Psi = \pm \sqrt{\frac{2Kx_e}{\epsilon_o \epsilon_r A (x_e - \chi)^2} \left(\frac{1}{(x_o - x_e)^2} - \frac{1}{(y_o + x_e)^2} \right)} \tag{1.14}$$

Where the sign determines whether negative or positive voltage is used. In order to satisfy the slope condition for positive region operation $x_e < \chi \leq x_o$. For the negative region χ needs to be less than x_e by very little. The slope of the device function is relatively large in the negative region, so selecting the intercept must be done carefully.

1.9.2 Positive Region Operation

Figure 1.7 and Figure 1.8 show the position output and voltage input for positive operation with $\chi = x_o$. The input voltage was also limited to be in the range $0 \leq V \leq 26V$ to ensure the system has only one (stable) equilibrium point. Large overshoots due to poor damping require either small steps or a ramp input in order to prevent the device from colliding with the stationary combs when $x = x_o$. Interestingly, the linear controller is mathematically equivalent to charge controllers like that proposed in [11] when $\chi = x_o$ and $y_o \rightarrow \infty$.

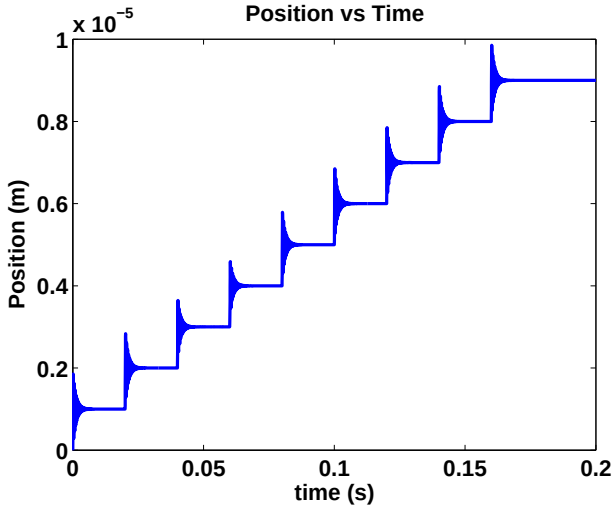

Figure 1.7: Output Position for Linear Controller, Positive Region

The choice of the x-intercept, χ, is somewhat arbitrary. However, in choosing χ, the following facts need to be considered; 1) an intercept closer to the equilibrium point yields larger potential barriers, 2) an intercept closer to x_o yields lower local stiffness.

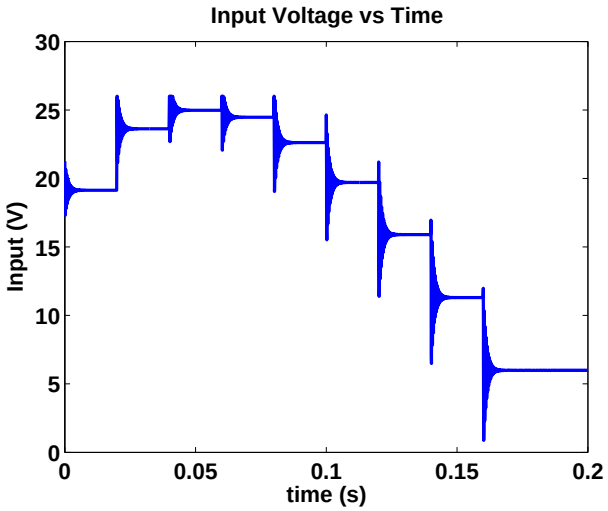

Figure 1.8: Input Voltage for Linear Controller, Positive Region

1.9.3 Negative Region Operation

Figure 1.9 and Figure 1.10 show the position output and voltage input for negative operation with $\chi = -y_o + \frac{2}{3}(y_o + x_e)$. Again, large overshoots due to poor damping require either small steps or a ramp input to prevent the device from colliding with the stationary combs $x = -y_o$.

Similar considerations to the positive region operation are required when choosing χ for negative region operation. The choice of χ also needs to satisfy the slope requirements for stable operation. One should also note that operation in the negative region will be somewhat more difficult than operation in the positive region due to the non-existence of equilibrium points in the region of $(0 > x \geq \frac{x_o^2 - y_o^2}{2(y_o + x_o)})$. Either an external force or dynamic excitation would have to be used to initialize the device for negative region operation. In Figure 1.9 the device was initialized at -10μm for example.

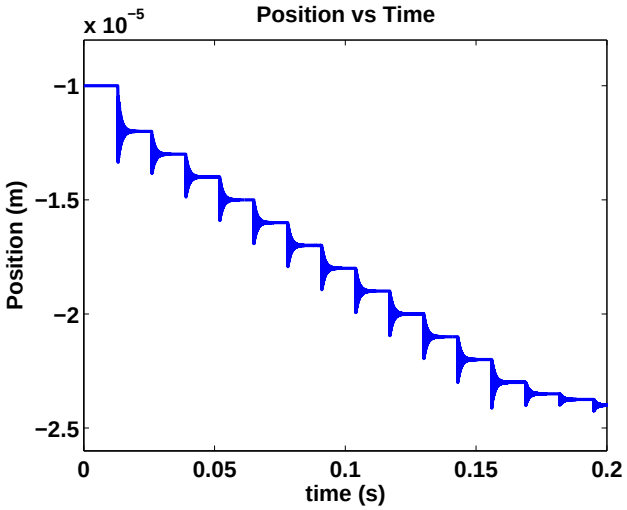

Figure 1.9: Output Position for Linear Controller, Negative Region

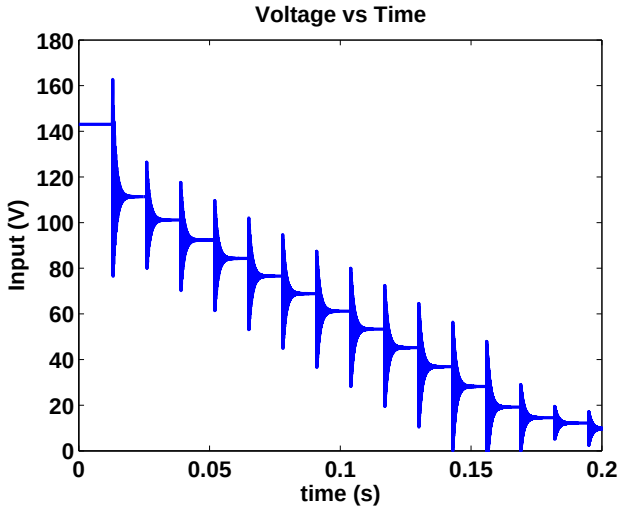

Figure 1.10: Input Voltage for Linear Controller, Negative Region

1.9.4 χ's Effect on Localized Stiffness

At this point it is beneficial to look at χ's effect on the localized stiffness of the system. Only positive region operation will be considered, however a similar argument can be made for negative region operation.

Figure 1.11 and Figure 1.12 show the device-plant functions and net force functions for 3 different intercept values respectively . The input functions are half parabolas with a saturation characteristic ($f_e \leq 26^2$ and $f_e = 0$ for $x \geq \chi$). With $\chi = x_o$ the input function is the widest parabola possible to establish one stable equilibrium point. As $\chi \rightarrow x_e$, the parabolas narrow and in the limiting case the feedback looks like a relay.

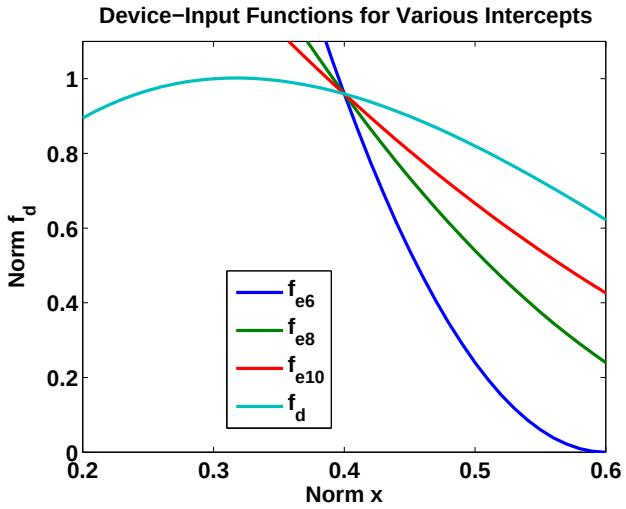

Figure 1.11: Device-Input Function for Various Chi Values

Figure 1.12 shows how the localized stiffness varies with the choice of χ. Linearizing the system about the equilibrium point, $\frac{dF}{dx}\Big|_{x_e} = k$. For a linear system k would be the spring constant or stiffness. The minimal system stiffness occurs when $\chi = x_o$, as χ decreases the stiffness increases and in the limiting case the stiffness approaches infinity.

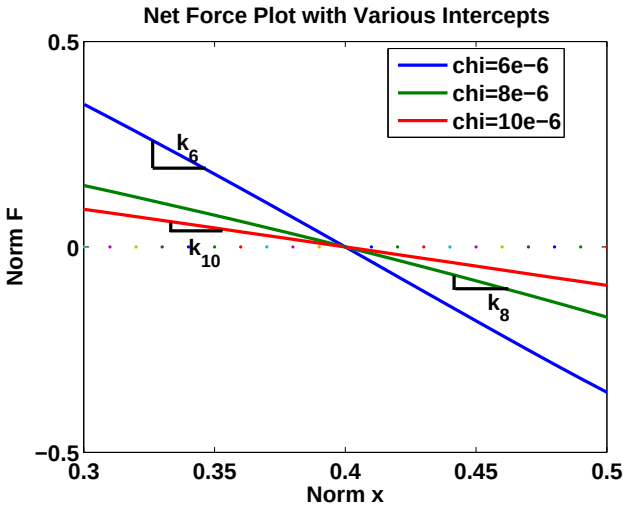

Figure 1.12: Net Force Functions for Various Chi Values

Because the localized stiffness of the system can be modified by choice of controller gains, a variable structure technique can be used to improve system performance.

Chapter 2

Variable Structure Technique

The control methodology up to this point does a good job of controlling the system under ideal conditions. Even under these circumstances, stabilizing the system can be problematic for systems with low mechanical damping. For zero damping, the system is only marginally stable. Because many MEMS devices have low damping and any real system has uncertainties, delays, and noise, a more robust control method may be required.

One solution is to use variable structure control. Variable structure control works by switching between 2 or more different control structures to improve performance. For example Figure 2.1 and Figure 2.2 show the phase response for the same system, the first having a feedback with low stiffness (low frequency), the second having a feedback with high stiffness (high frequency).

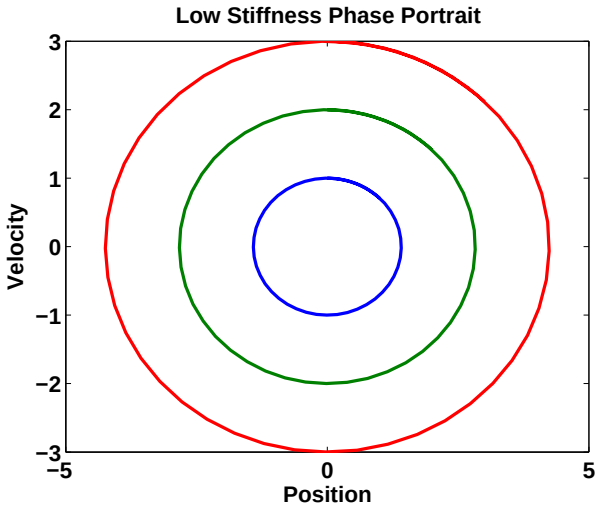

Figure 2.1: Low Stiffness Phase Portrait

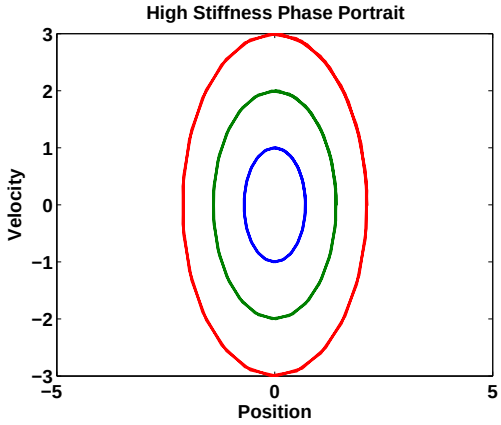

Figure 2.2: High Stiffness Phase Portrait

Both systems are marginally stable. However, by switching between the two structures the system becomes asymptotically stable as shown in Figure 2.3. The switching criteria is to use the high stiffness system if the position-velocity product is greater than 0, otherwise the low stiffness system is used.

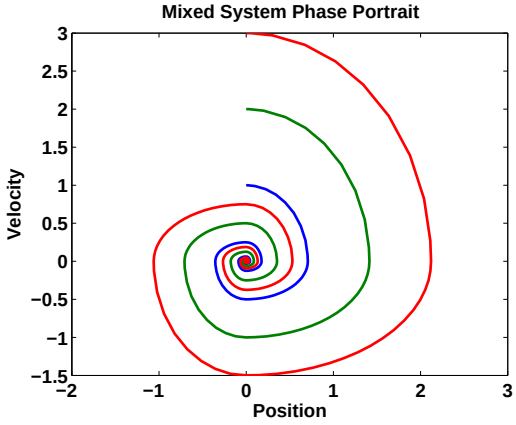

Figure 2.3: Mixed System Phase Portrait

2.1 Available Structures

There are 6 different types of structures available for second order system equilibrium points. By linearizing the system an the equilibrium point and determining the eigenvalues of the linearized system the type can be determined. Because the damping coefficient is so low for the GCA system, it can be ignored without affecting the analysis. With zero damping, there are only 2 possible structures to switch between, an unstable saddle point and the marginally stable center point. This fact can be attributed to the physics of the system, forces either pushing the actuator away from or toward the equilibrium point. Figure 2.4 shows the phase portrait for the system with a constant input voltage with the two types of equilibrium points.

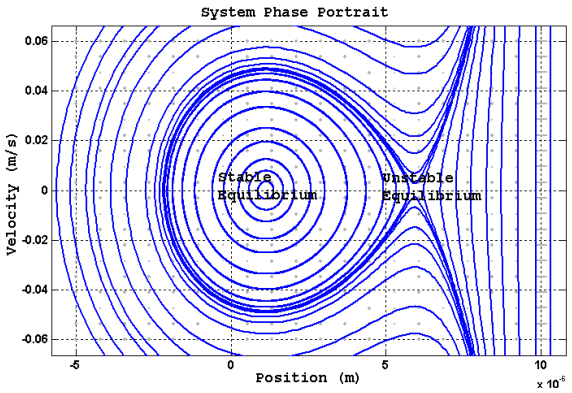

Figure 2.4: Constant Voltage, Zero Damping Phase Portrait

2.2 GCA Variable Structure Controllers

Both the stable and unstable equilibrium behavior can be used to implement variable structure control for the GCA system. Switching between two marginally stable systems works similarly to the controller shown in Figure 2.3, where the system stiffness can be

varied as discussed previously. This forced damping method can be implemented using 2 or 4 different structures. Using 2 structures improves damping when the system dynamics are well known. Using 4 structures also improves damping and also makes the system more robust in cases where there are many unknowns present.

Switching between a marginally stable structure and an unstable structure results in a sliding mode controller, where the phase trajectory is forced toward the switching surface. Again, 2 or 4 structures can be used, with similar reasons as stated above. Under some circumstances, this type of variable structure controller outperforms the forced damping type.

2.2.1 Stable-Stable (Forced Damping) Switching

To demonstrate how the forced damping controller improves system response absent of system uncertainties the linear controller previously described is used. The high stiffness structure uses $\chi = x_e + \frac{x_o - x_e}{10}$, the low stiffness structure uses $\chi = x_o$. The switch sample time was set at 1 μs for simulations.

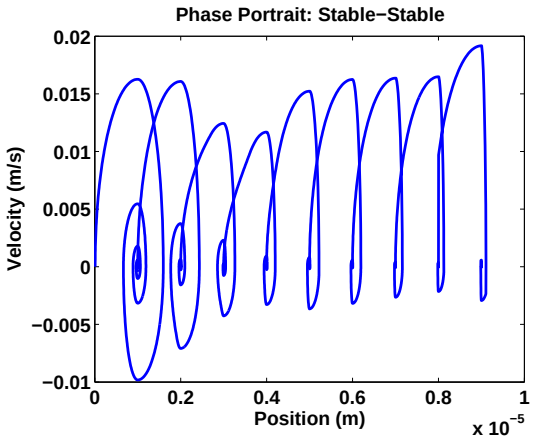

Figure 2.5: Stable-Stable Phase Portrait

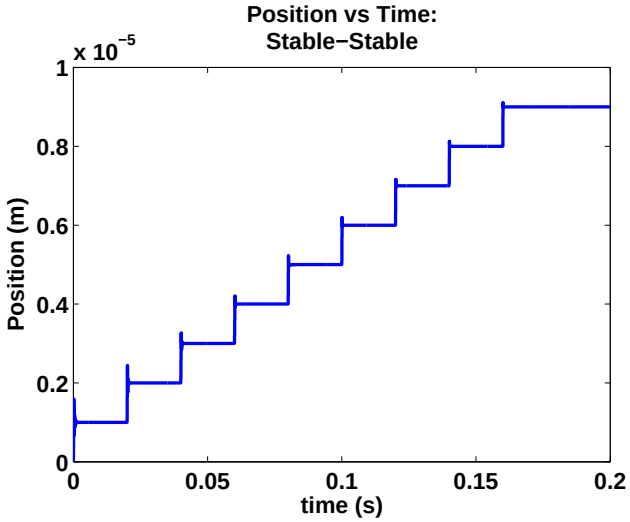

Figure 2.6: Stable-Stable: Position vs Time

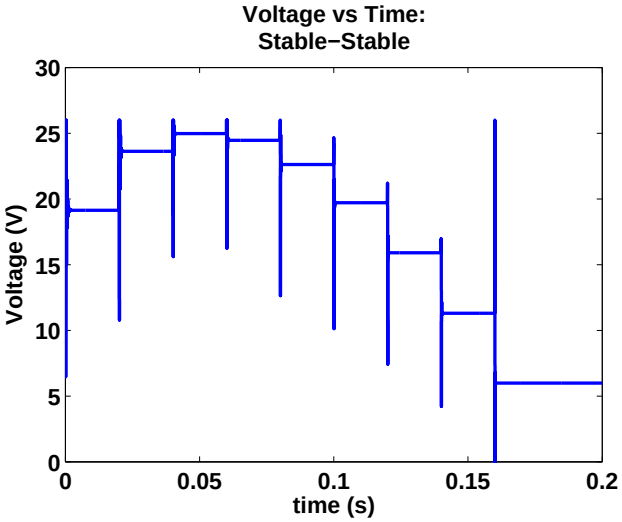

Figure 2.7: Stable-Stable: Control Voltage vs Time

2.2.2 Stable-Unstable (Sliding Mode) Switching

To demonstrate how the sliding mode controller improves system response absent of system uncertainties the linear controller previously described is used. The stable structure uses $\chi = x_e + \frac{x_o - x_e}{4}$, the unstable structure uses $\chi = 5x_o$. The switch sample time was set at 1 μs for simulations.

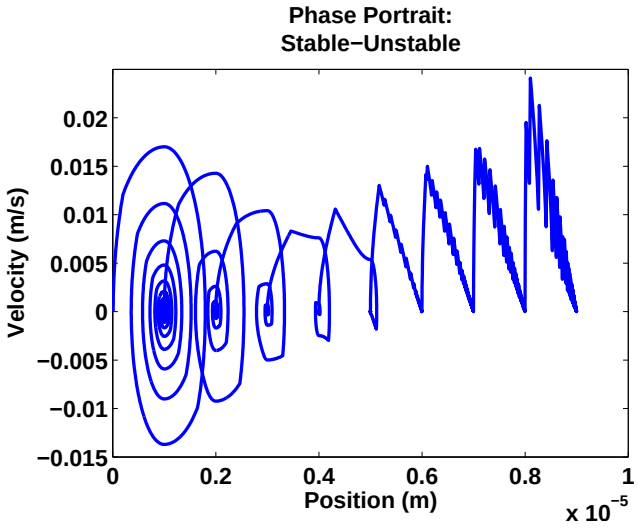

Figure 2.8: Stable-Unstable Phase Portrait

Figure 2.8 shows that the system only reaches the sliding mode on the last few equilibrium points. The structures chosen form a hybrid system, partially forced-damping, partially sliding-mode, depending on where in the travel range the device is located. The switching surface also needed to be modified to ensure proper controller performance.

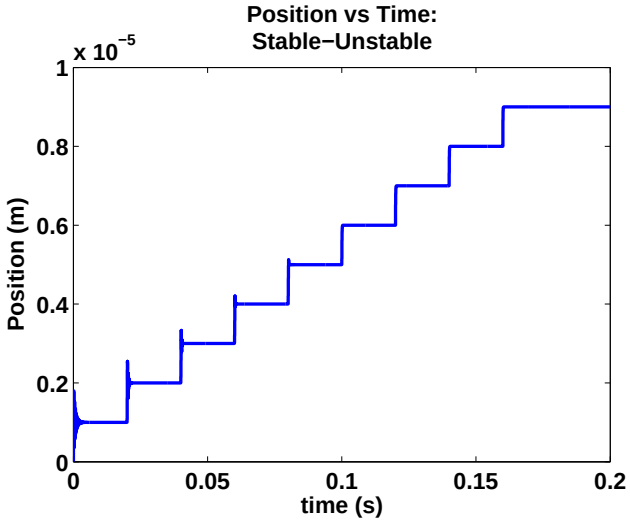

Figure 2.9: Stable-Unstable: Postion vs Time

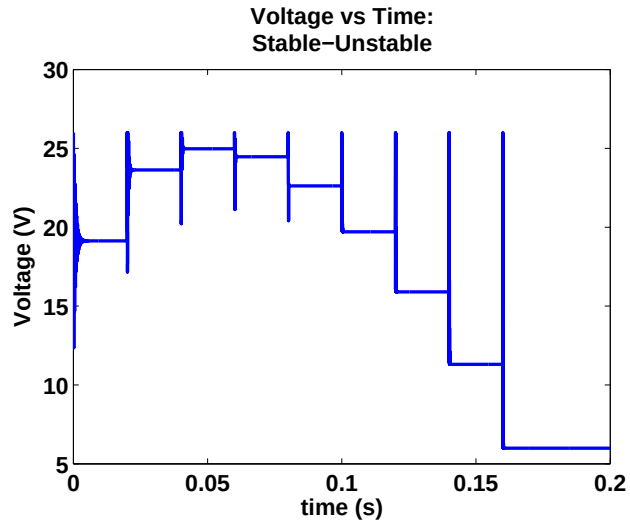

Figure 2.10: Stable-Unstable: Control Voltage vs Time

2.2.3 Switching Surface Considerations

For the forced-damping controller, only the position-velocity product needed to be known to determine if the high-stiffness or low-stiffness structure was engaged. In order to make the sliding-mode controller work properly the switching criteria had to be slightly modified. For the stable structure to be engaged:

$$(mx_1 + x_2)x_1 > 0 \tag{2.1}$$

Where $m \geq 0$ is the slope of the switching surface. Otherwise the unstable structure was engaged. For the stable-unstable method described in the last section $m = 15000$ was chosen using trial and error. A more rigorous method of determining the correct slope to ensure a sliding mode would be forcing $\sigma\dot{\sigma} < 0$ where the switching surface is $\sigma = mx_1 + x_2$. However, understanding the shape of the phase portraits of both structures is less cumbersome than doing the math.

The quadrant switching ($m = 0$) used with the stable-stable controller could also be modified. There might be certain cases where such switching is beneficial, although theoretically it is not necessary.

Chapter 3

Adaptive Controller

The control methods described thus far have assumed perfect knowledge of system dynamics. Due to fabrication imperfections, modeling uncertainties, and other similar effects, the system is never perfectly known. For example, deep reactive ion etching is one of the best fabrication techniques to generate vertical side-walls. However, even small angular errors can affect the capacitance, [12] notes that even the relatively small aspect angle of $\alpha < 1^\circ$ can have a dramatic effect on capacitance. The equation for a simple (not quite) parallel plate capacitor is given:

$$\frac{C(\alpha)}{C(0)} = \frac{d}{2T\ \tan\alpha} \ln \frac{d}{d - 2T\ \tan\alpha} \tag{3.1}$$

Where d top side gap width, α is the under-etch angle, and T is the depth of the etch (device thickness). An attempt was made to determine exactly how (3.1) modifies the device function, but the form of the equation makes that analysis very difficult. Despite this fact, it should be clear that the effects of aspect ratios, fringe fields, and other effects generate some relatively large uncertainties in the device function, so any proposed controller should be quite robust. The linear controller works well because the input function slope and intercept can be varied to compensate for any uncertainties.

$$V(x) = \Psi(x - \chi) \tag{3.2}$$

Solving for Ψ is not possible when the device function is unknown. To compensate for this a simple adaptive algorithm can be implemented using a PI (proportional-integral) method:

$$\Psi = P\left(x_e - x + I\int_0^t x_e - x \; d\tau\right) \tag{3.3}$$

In order for the adaptive controller to work properly, natural damping must be present since the controller cannot force damping like the controllers previously discussed. In cases with low damping the adaptive gains need to be decreased so that the natural damping has time to eliminate transients. Simulations use the damping given in Table 1.1, and an intercept of $\chi = x_o$, and PI gains of $(1 \times 10^{12}, 1 \times 10^{3})$ respectively.

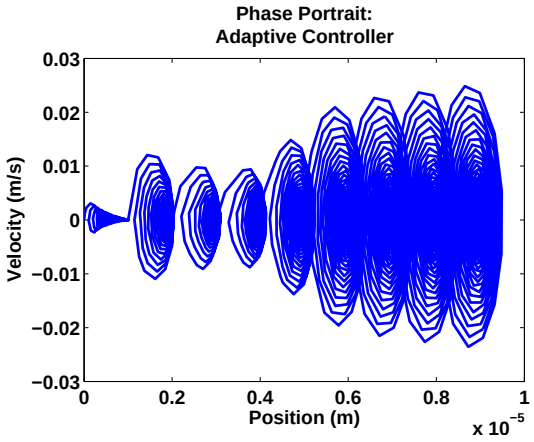

Figure 3.1: Adaptive Controller Phase Portrait

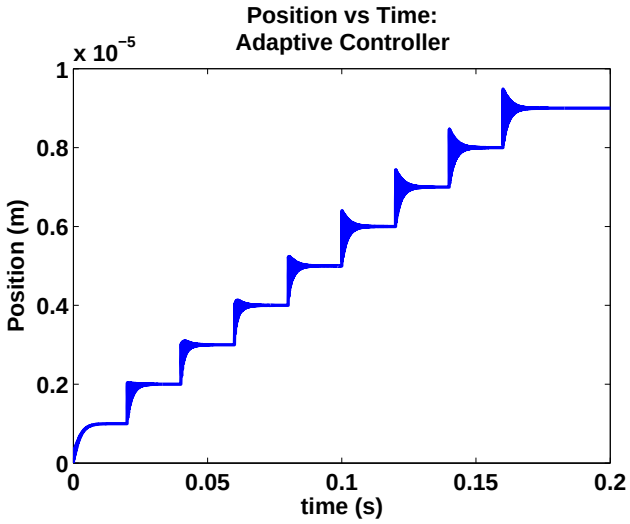

Figure 3.2: Adaptive Controller: Position vs Time

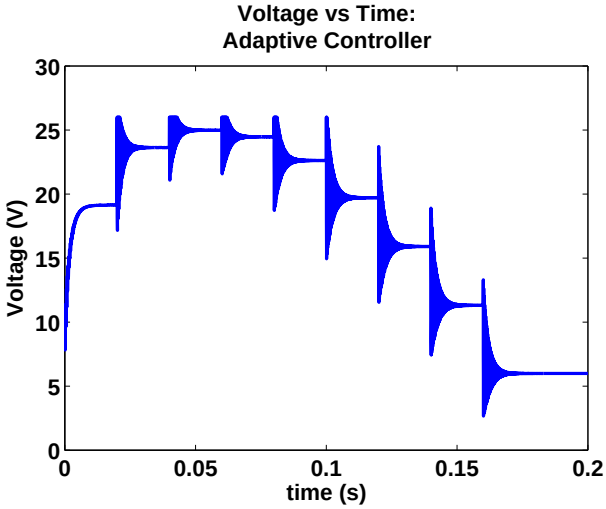

Figure 3.3: Adaptive Controller: Control Voltage vs Time

Table 3.1: Approximate parameter values for robustness study

Variable	**Parameter**	**Value**	**Units**
m	mass	3.561×10^{-7}	kg
B	damping	2.39×10^{-4}	N-sec/m
ϵ_o	free space permittivity	8.854×10^{-12}	F/m
ϵ_r	relative permittivity	1	NA
A	area	5.042×10^{-6}	m^2
x_o	nominal small gap	9.563	μm
y_o	nominal large gap	27.23	μm
K	spring constant	115.2	N/m

3.1 Robustness Comparison

In order to compare the robustness of the different controllers discussed, the controller parameters were randomly varied by $\pm 20\%$. Control signals were generated using the parameters given in Table 3.1. System dynamics were still set by the parameter values given in Table 1.1. Figure 3.4 and Figure 3.5 show the output responses and phase portraits for all three controllers respectively.

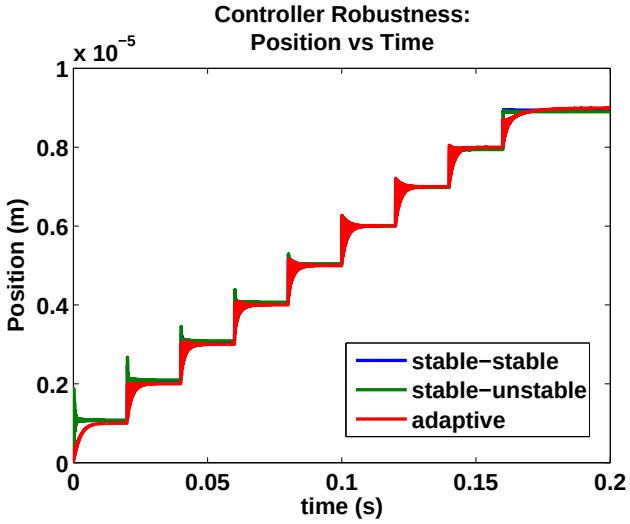

Figure 3.4: Robustness Study: Position vs Time

While the adaptive controller provides zero steady state error, the dynamic response leaves something to be desired. The two variable structure controllers respond quickly, but have steady state errors. The reason being the variable structure controllers switch between two structures with feedback functions that intercept the device function at two different locations. For any desired equilibrium point, the adaptive algorithm has only one equilibrium point it settles upon, however, the variable structure algorithms have two equilibrium points they switch between. This switching causes a very complicated dynamic that can cause instability if the equilibrium points are too far away from each other.

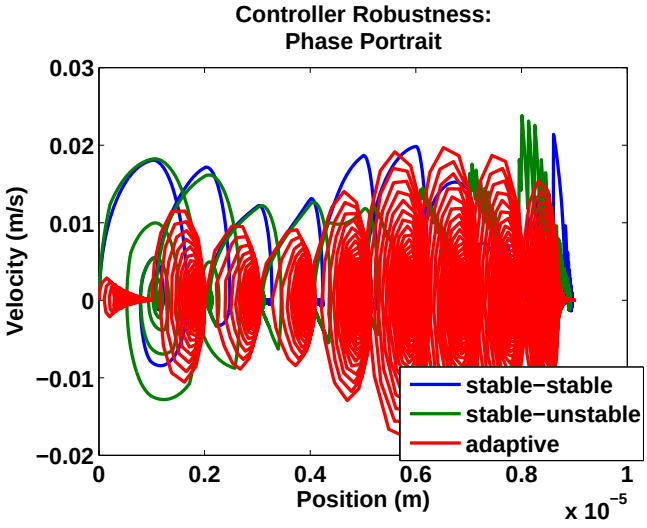

Figure 3.5: Robustness Study: Phase Portrait

Chapter 4

Device Function Design

Considering all the aspects that would need to be addressed when designing a MEMS device is too much to cover here. However, there are a handful of items to keep in mind when designing a system to be controlled using feedback. Once again the GCA will be used for example, but similar arguments can be make for any nonlinear electrostatic device. The input-device function for the GCA can be written:

$$V^2 = \frac{2F_m}{\epsilon_o \epsilon_r A} \left(\frac{1}{(x_o - x)^2} - \frac{1}{(y_o + x)^2} \right)^{-1} \tag{4.1}$$

Where $F_m = Kx$ is the mechanical force for the typical linear spring model. When designing the spring, minimizing the spring constant, K, has two benefits. The first benefit is that it minimizes the actuation voltage required for both open loop and closed loop operation. The second benefit is it minimizes the forces (mechanical and electrical) acting on the system mass when using feedback control. If there are any time delays in the loop, then smaller forces prevent instability due to slower system dynamics. Increasing the mass or inertia of the device has a similar effect. However, the resultant lowering of the natural frequency of the device can make it susceptible to external vibration [13].

4.1 Nonlinear Springs

Theoretically, the open loop travel range can be extended by offsetting the electrical force nonlinearity with a mechanical force nonlinearity. This can be done by designing the mechanical force curve $F_m(x)$ so that:

$$\frac{d}{dx}\frac{2F_m(x)}{\epsilon_o \epsilon_r A}\left(\frac{1}{(x_o - x)^2} - \frac{1}{(y_o + x)^2}\right)^{-1} > 0 \tag{4.2}$$

One possible solution is:

$$F_m(x) = \begin{cases} Kx & (0 < x < x_l) \\ \gamma(x - \alpha)\left(\frac{1}{(x_o - x)^2} - \frac{1}{(y_o + x)^2}\right) & (x_l < x < x_o) \end{cases} \tag{4.3}$$

Where x_l is in the stable range of open loop operation for the linear mechanical force. The variables γ and α are used to ensure continuity in the force function and set the slope of the device function. To ensure force continuity:

$$\alpha = x_l - \frac{Kx_l}{\gamma}\left(\frac{1}{(x_o - x_l)^2} - \frac{1}{(y_o + x_l)^2}\right)^{-1} \tag{4.4}$$

Using the GCA device as a template, a nonlinear spring system was simulated for $x_l = 3\mu$m, $\gamma = 7.5 \times 10^{-9}$Nm, and $\alpha = 2.46\mu$m.

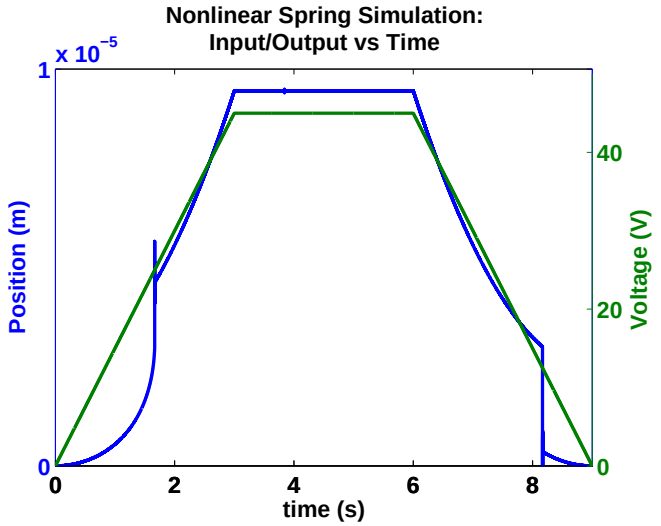

Figure 4.1: System Response with Nonlinear Spring

Once $F_m(x)$ has been determined, the nonlinear spring has to be designed. The design is based on determining an interference profile to prevent beam deflection once the displacement reaches a set value. An iterative method was used along with standard beam theory. Using the beam variables from the GCA example where the beam length $L = 1200\mu$m, the beam width $w = 15\mu$m, and the beam depth $d = 75\mu$m. The modulus of elasticity for silicon is $E = 176$GPa. Using the beam element in Figure 4.2 the displacement and slope equations can be determined.

$$y(l) = \frac{F}{EI}\left[\frac{1}{6}l^3 - \frac{1}{4}Ll^2\right] + sl\left[1 - \frac{l}{2L}\right] + y_o \tag{4.5}$$

$$\frac{dy(l)}{dl} = \frac{F}{EI}\left[\frac{1}{2}l^2 - \frac{1}{2}Ll\right] + s\left[1 - \frac{l}{L}\right] \tag{4.6}$$

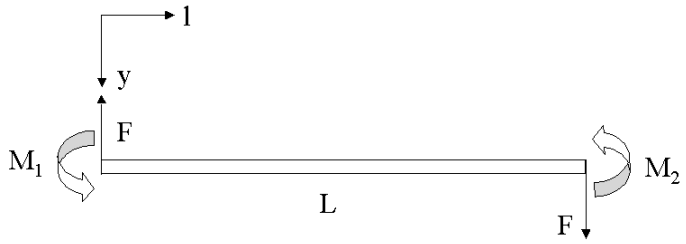

Figure 4.2: Beam Element for Nonlinear Spring Design

Where $y(l)$ is the beam deflection along the beam element, y_o and s are the element deflection and slope at the left end of the element, and EI is the sectional stiffness of the beam. The iteration method starts with determining the deflection and slope at the first interference point using the force from equation (4.3) at $x = x_l$. These new boundary conditions are then applied to a new element with a desired force from equation (4.3) making sure the displacement at the right end of the beam matches the displacement input to the force equation. The results are shown in Figure 4.3. The blue line is the interference profile, the black lines are the beam profiles for different mass deflections, and the red line is an example of a beam profile without interference (linear spring).

4.2 Implementation Issues

Modifying the device function using nonlinear springs looks promising because the travel range is extended to the entire range of motion in open loop operation. However, implementation would be problematic. First of all, higher stresses might cause mechanical failure in the beams. Secondly, device function uncertainty would make designing the interference profile difficult. A more aggressive interference profile could be designed to compensate (say by shifting the entire profile towards the proof mass), but this would

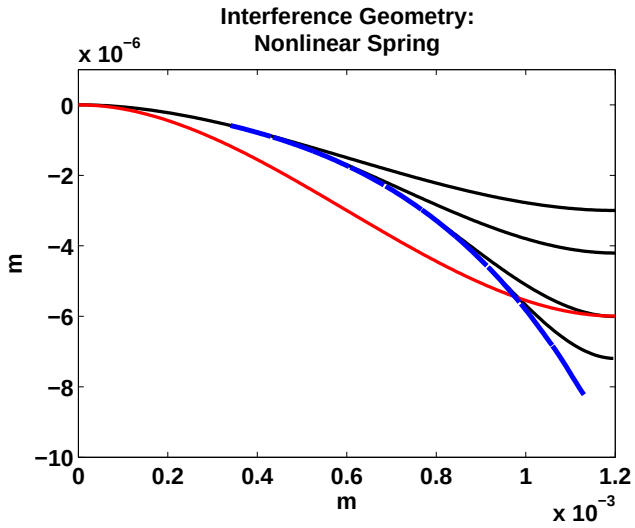

Figure 4.3: Interference and Deflection Profiles

likely increase the actuation voltage. Thirdly, depending on fabrication technology, not all nonlinear electrostatic devices could use interference profiles.

Planar SOI (silicon on insulator) devices would be prime candidates for implementation (like the GCA example). However, even this technology would have implementation difficulties. Photolithography (mask) restrictions would limit the resolution of the interference profile. Fabrication issues would further degrade the profiles (over-etching, etc.). Stiction could also be a problem, a continuous interference profile providing a large contact area. The profile could be approximated using discrete contact points, but even this causes problems. Discrete contact points can cause an intermediate pull-in phenomenon. Figure 4.4 shows the device function for such an arrangement. When the slope of the device function is zero a localized pull-in occurs to the next intersection point. This would cause a complicated hysteresis behavior that would extend the travel range in a limited manner with erratic behavior near pull-in locations.

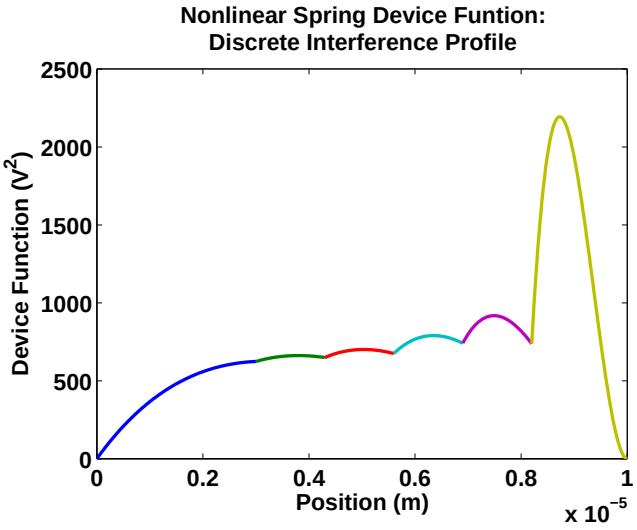

Figure 4.4: Discrete Nonlinear Spring Device Function

Other methods have been shown to produce nonlinear mechanical springs. For example, instead of using contact forces from an interference profile, additional electrodes could be implemented to create forces on the beam that changes the spring characteristic. Another example is given in [14], where controlling motion in a cross direction effects the spring constant in the direction of interest.

Chapter 5

Extension to Other Systems

In order to demonstrate the scope of the method, it will be used to demonstrate how the series capacitor method extends the travel range of the GCA example. The method will also be applied to a tilt actuator example.

5.1 Series Capacitor Method

The series capacitor method is an open loop approach to extend the travel range of nonlinear electrostatic MEMS actuators. The method works by forming a voltage divider that acts like a closed loop system. The voltage across the device, V_d, is given:

$$V_d = \frac{V_s}{1 + \frac{C_d}{C_s}} \tag{5.1}$$

Where V_s is the supply voltage across the series pair, C_d is the variable capacitance of the device, and C_s is the series capacitor. Using a series capacitor of 1/4 the nominal capacitance of the device:

$$\begin{aligned} C_s &= \frac{\epsilon_o \epsilon_r A}{4}\left(\frac{1}{x_o} + \frac{1}{y_o}\right) \\ V_d(x) &= \frac{V_s(x_o - x)(y_o + x)}{(x_o - x)(y_o + x) + 4x_o y_o} \end{aligned} \tag{5.2}$$

Where $V_d^2(x)$ is the input function that meets the slope criteria previously discussed for stable equilibrium points. Figure 5.1 is the device-input plot and Figure 5.2 is the net force plot for 3 different supply voltages.

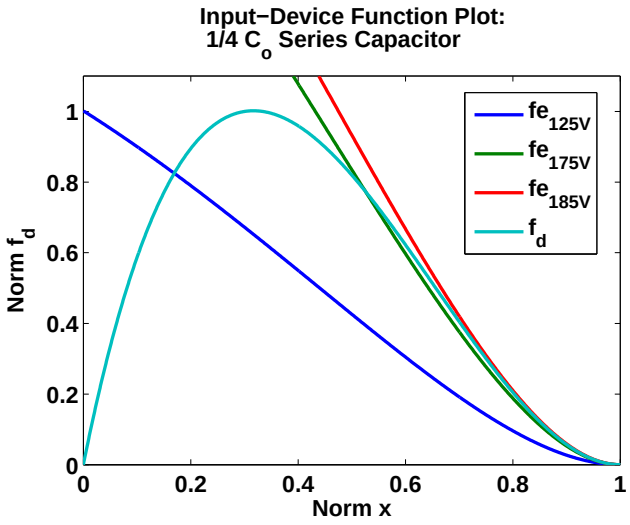

Figure 5.1: Series Capacitor Device-Input Plot

The plots show that the series capacitor shown is too large to provide full range of motion. Decreasing the value of the series capacitor would increase the travel range, but at the cost of higher actuation voltage. Using the series capacitance given, the actuation voltages are relatively high, pull-in occurring around $V_s = 182.5$V at a displacement roughly $x = 8\mu$m. Work has been done by Dr. Robert N. Dean and Dr. John Y. Hung at Auburn University to improve the series capacitor feedback using analog circuitry to increase travel range without increasing the supply voltage. Improved feedback has also been reported using MOS capacitors [15].

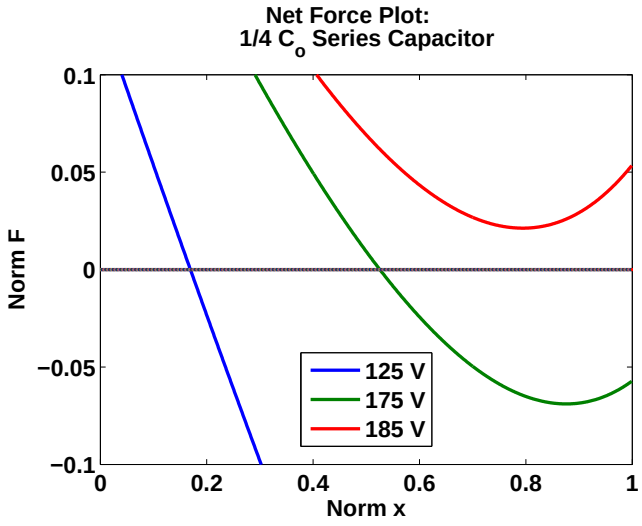

Figure 5.2: Series Capacitor Net Force Plot

5.2 Torsional Devices

The method can also be applied to torsional devices. The only functional difference between a torsional device with GCA is the electrostatic force nonlinearity. The capacitance of a torsional device is given [16] as:

$$C(\theta) = \frac{\epsilon_o \epsilon_r h}{\theta} \ln\left(\frac{a+b}{a}\right) \tag{5.3}$$

Where θ is the angle between the two electrodes, a is the lesser radial electrode dimension, b is the electrode length, and h is the out of plane dimension of the electrode. For most torsional devices, rotations are assumed to occur about a fixed point located a gap distance, g, above the stationary electrode. In order for this fixed point to remain constant:

$$a(\theta) = \frac{g}{\sin\theta} - b \tag{5.4}$$

The electrostatic torque can then be found:

$$\begin{aligned} T_e(\theta) &= \frac{1}{2}V^2\frac{d}{d\theta}C(\theta) \\ \frac{d}{d\theta}C(\theta) &= \frac{\epsilon_o\epsilon_r h}{\theta}\left[\frac{b\ \cos\theta}{g - b\ \sin\theta} - \frac{1}{\theta}\ln\left(1 + \frac{b\ \sin\theta}{g - b\ \sin\theta}\right)\right] \end{aligned} \tag{5.5}$$

Figure 5.3 and Figure 5.4 show the normalized device-input plots and net torque plots respectively. The shape of the device function does differ slightly from that of the GCA, but the same slope conditions apply for stability.

The same controller used for the GCA can be used for a torsional device:

$$V(\theta) = \Psi(\theta - \Theta) \tag{5.6}$$

Setting Θ to be the maximum angular displacement of the device, the normalized device-input plot and net torque plots were generated using various values of Ψ.

Like the GCA, the travel range of a torsional actuator can be extended to the full range using the linear controller. No further analysis has be done, however the variable structure and adaptive techniques described earlier could be applied to torsional systems.

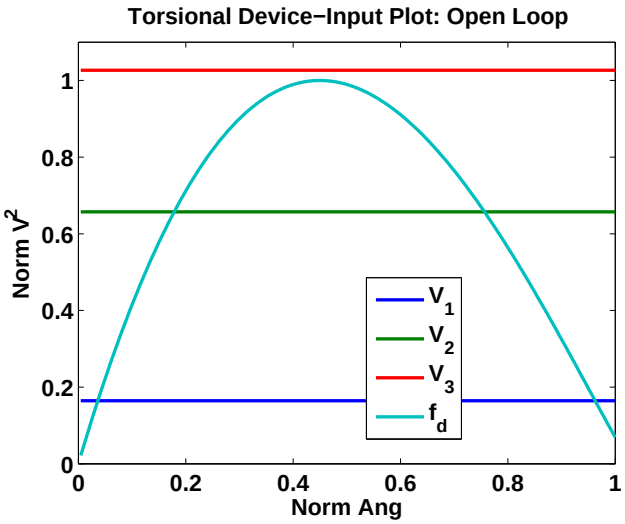

Figure 5.3: Torsional Device-Input Plot: Open Loop

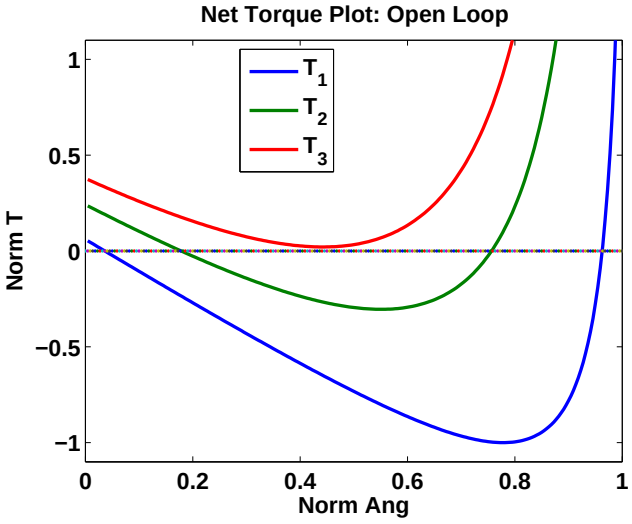

Figure 5.4: Net Torque Plot: Open Loop

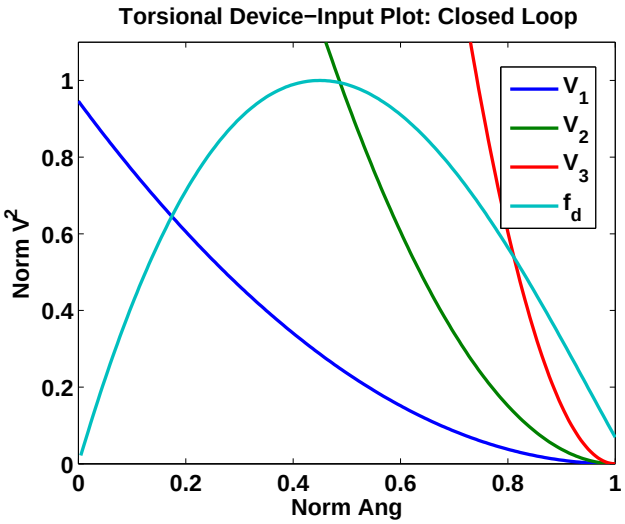

Figure 5.5: Torsional Device-Input Plot: Closed Loop

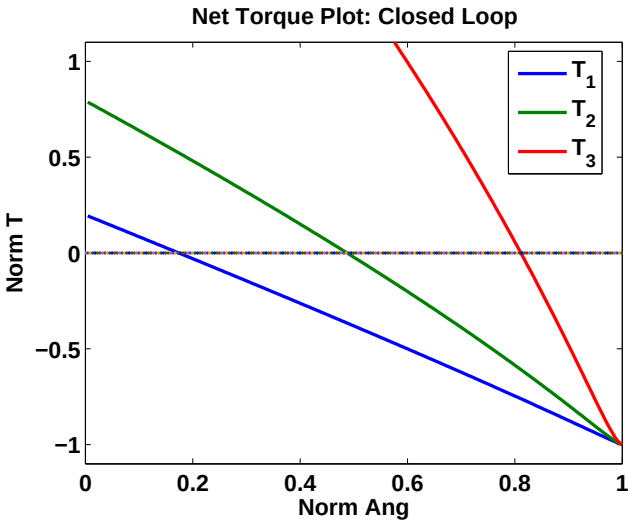

Figure 5.6: Net Torque Plot: Closed Loop

Chapter 6

Conclusion and Discussion

6.1 Overview

Static stability is at the heart of the method discussed. Using static stability, the device-input formulation was developed by setting the derivative terms to zero in the governing equation and isolating the input voltage term V^2 to one side of the resultant equality. The utility of the method rests in the fact that the input voltage can be manipulated given any device to ensure static stability. The method also provides insight into how the device itself can be designed to improve both open and closed loop performance.

Once the device-input formulation was established, a simple, linear controller was proposed. This controller guaranteed the existence of only one stable equilibrium point for the system as long as $x_e < \chi \leq x_o$ (positive operation). An adaptive controller was proposed based on the linear controller the can adapt to the correct slope, Ψ, for a given intercept with no additional system information required.

The proposed linear controller was also used to develop two variable structure methods to improve system performance. Controller gains determined the structures that were switched between. The first variable structure proposed used two stable systems to force damping. By switching between two systems with high or low localized stiffness overall performance was improved dramatically. The second variable structure proposed used stable and unstable systems to form a hybrid sliding mode controller. Switching was done between two input functions, the first where $x_e < \chi \leq x_o$, had only one stable equilibrium point.

The second, where $\chi >> x_o$ had two equilibrium points, one stable, one unstable. The reason the system is best described as hybrid is because for equilibrium points where $\frac{df_d}{dx} > 0$ a stable-stable switching is present, where $\frac{df_d}{dx} \leq 0$ stable-unstable switching is present and a sliding mode controller was observed.

Next, focus was shifted from the input function to the device function. Design considerations for devices that are intended to operate under closed loop control were covered. Then, a method that extends the positive slope range of the device function was proposed. Extending the positive slope range of the device function extends the open loop travel range by offsetting the electrostatic nonlinearity with a mechanical nonlinearity.

After showing how the method can be used to design controllers and devices based on the GCA example, the method was extended to other MEMS in order to demonstrate the utility of the method. The first system was the GCA in series with a dummy capacitor. In open loop, this system extends the travel range of the device at the cost of higher actuation voltage. The second system was a 1-dimensional torsional actuator. The device function was determined and a similar analysis showed that input functions just like the GCA's could be used to extend the travel range of the system. Variable structure and adaptive methods could also be applied to the torsional actuator.

Aside from the numerous benefits of the method, there are many issues that would need to be addressed in any future work. The following sections attempt to introduce the most predominate of these issues.

6.2 Output vs State Feedback

The bulk of the method relies on output feedback, assuming the system output is the displacement of the actuator. There are two reasons for this: 1) the static stability analysis only requires this type of feedback, and 2) velocity measurements can be difficult on this scale [17]. Parasitic capacitance, fabrication uncertainties, and measurement issues make position measurement difficult enough. The only proposed controller that requires accurate velocity measurement is the sliding mode controller where the switching surface has been rotated in the phase plane. The other forced-damping technique only required the sign of the velocity-position product, which is easier to estimate. The method is robust in terms of workability without accurate velocity information. However, the output measured from most of these devices is in terms of capacitance, not position. While the transformation between capacitance and position should be fairly simple for 1-1 relationships, it might be enlightening to formulate the device-input functions where capacitance is the independent variable. This is one potential direction of future research.

6.3 Multi-Dimensional Actuators

It would be interesting to apply the method to multi-dimensional devices such as micro-mirrors with two rotational axes. Cross axis coupling could make the work-energy formulation of the electrostatic torques difficult, but it should be possible. An additional problem would be choosing the number of actuation electrodes. With luck the method might be powerful enough to allow full range of motion with only 4 electrodes. Instinctively, it makes sense that the device function would be a surface with the two independent variables being the rotation axes. Input function(s) would also likely be surface(s) over the two rotation

variables, however the input-output function relations for equilibrium and stability are not immediately clear. Research along these lines would be interesting, however, there is no guarantee this method would work for systems with multiple degrees of freedom.

6.4 Final Discussion

Overall, the methods described are based on static equilibrium analysis. These methods were developed in a somewhat ad-hoc manner, with the intent to tie them into a more traditional type of control system analysis. However, as the method developed, the choice was made to keep things simple by not complicating the analysis using Lyapunov or a linearization technique. Static stability based controllers ensure that for a given displacement, a constant voltage is converged upon. While there are cases where a state of dynamic stability can be reached with wild input voltage fluctuations (like the switching controllers with device function uncertainty), thorough understanding of these complex dynamics are unnecessary for slow actuation requirements.

Most implementation aspects have not been addressed. Quantization and time delays do cause considerable problems for the designed GCA device. Simulations show that these problems could be reduced by increasing the mass of the device, or decreasing the stiffness. Another aspect that has not been modeled is the RC dynamics of the system, finite charge rates will no doubt effect overall system dynamics.

The methods described show much promise, but additional work needs to be done. Implementation, using analog or digital circuitry, is the biggest hurdle. Implementation issues will likely present problems not addressed in this analysis, however, these methods should improve performance for most devices.

Bibliography

[1] B. Borovic, F. L. Lewis, W. McCulley, A. Q. Liu, E. S. Kolesar, and D. O. Popa, "Control issues for microlectromechanical systems," *IEEE Control Systems Magazine*, vol. 26, no. 2, pp. 18–21, April 2006.

[2] C. T.-C. Nguyen, "Frequency-selective MEMS for miniaturized low-power communication devices," *IEEE Transactions on Microwave Theory and Techniques*, vol. 47, no. 8, pp. 1486–1503, August 1999.

[3] E. S. Hung and S. D. Senturia, "Extending the travel range of analog-tuned electrostatic actuators," *Journal of Microelectromechanical Systems*, vol. 8, no. 4, pp. 497–505, December 1999.

[4] L. A. Rocha, E. Cretu, and R. F. Wolffenbuttel, "Using dynamic voltage drive in a parallel-plate electrostatic actuator for full-gap travel range and positioning," *IEEE Journal of Microelectromechanical Systems*, vol. 15, no. 1, pp. 69–83, February 2006.

[5] J. Chiou and Y. Lin, "A novel capacitance control design of tunable capacitor using multiple electrostatic driving electrodes," *Nanoelectronics and Giga-Scale Syatems (Special Session)*, no. M3.1, October 2001.

[6] E. S. Hung and I. Stephen D. Senturia, Fellow, "Extending the travel range of analog-tuned electrostatic actuators," *IEEE Journal of Microelectromechanical Systems*, vol. 8, no. 4, pp. 497–505, December 1999.

[7] J. I. Seeger and B. E. Boser, "Charge control of parallel-plate, electrostatic actuator and the tip-in instability," *Journal of Microelectromechanical Systems*, vol. 12, no. 5, pp. 656–671, October 2003.

[8] J. Chen, W. Weingartner, A. Azarov, and R. C. Giles, "Tilt-angle stabilization of electrostatically actuated micromechanical mirrors beyond the pull-in point," *IEEE Journal of Microelectromechanical Systems*, vol. 13, no. 6, pp. 988–997, December 2004.

[9] D. H. S. Maithripala, J. M. Berg, and W. P. Dayawansa, "Nonlinear dynamic output feedback stabilization of electrostatically actuated mems," in *Proceedings of 42nd IEEE Conference on Decision and Control*, vol. 1, December 2003, pp. 61–66.

[10] J. E. Rogers, P. M. Ozmun, J. Y. Hung, and R. N. Dean, "Bi-directional gap closing MEMS actuator using timing and control techniques," in *Proceedings of 32nd Annual Conference of IEEE Industrial Electronics Society*, November 2006, pp. 3149–3154.

[11] D. H. S. Maithripala, J. M. Berg, and W. P. Dayawansa, "Capacitive stabilization of an electrostatic actuator: output feedback viewpoint," in *Proceedings of the 2003 Americal Control Conference*, vol. 5, June 2003, pp. 4053–4058.

[12] B. Borovic, F. L. Lewis, A. Q. Liu, E. S. Kolesar, and D. Popa, "The lateral instability problem in electrostatic comb drive actuators: modeling and feedback control," *Journal of Micromechanics and Microengineering*, vol. 16, pp. 1233–1241, 2006.

[13] R. Dean, G. Flowers, S. Hodel, K. MacAllister, R. Horvath, A. Matras, G. Robertson, and R. Glover, "Vibration isolation of mems sensors for aerospace applications," in *IMAPS International Conference and Exhibition on Advanced Packaging and Systems*, Reno, NV, March 2002, pp. 166–170.

[14] M. T.-K. Hou, G. K.-W. Huang, J.-Y. Huang, K.-M. Liao, R. Chen, and J.-L. A. Yeh, "Extending displacements of comb drive actuators by adding secondary comb electrodes," *Journal of Mircomechanics and Microengineering*, vol. 16, no. 16, pp. 684–691, February 2006.

[15] J. I. Seeger and S. B. Crary, "Stabilization of electrostatically actuated mechanical devices," in *Proceedings of the Ninth International Conference Solid State Sensors and Actuators*, Chicago, IL, June 1997, pp. 1133–1136.

[16] R. N. Dean, J. Y. Hung, and B. M. Wilamowski, "Advanced controllers for microelectromechanical actuators," in *Proceedings of 2005 IEEE International Conference on Industrial Technology*, Kowloon, Hong Kong, December 14-16, 2005.

[17] R. N. Dean, G. Flowers, R. Horvath, N. Sanders, A. S. Hodel, J. Y. Hung, and T. A. Roppel, "A relative velocity sensor for improved electrostatic parallel plate actuator control," *IEEE Sensors Journal*, vol. 7, no. 4, pp. 496–561, April 2007.